JOURNAL OF Applied Polymer SCIENCE

Preparation and Electrochemical Performances of Porous Polypyrrole Film by Interfacial Polymerization

Mingxia Shen,[1] Yongqin Han,[1] Xiaochen Lin,[2] Bing Ding,[2] Luojiang Zhang,[2] Xiaogang Zhang[2]

[1]College of Mechanics & Materials, Hohai University, Nanjing 210098, People's Republic of China

[2]College of Material Science & Engineering, Nanjing University of Aeronautics and Astronautics, Nanjing 210016, People's Republic of China

Correspondence to: Y. Han (E-mail: yongqinhan@126.com) or X. Zhang (E-mail: azhangxg@163.com)

ABSTRACT: In this study, porous polypyrrole (PPy) film was synthesized by facile interfacial polymerization using ionic liquid as oxidant. The morphology of PPys changed from dense microspherical/nanospherical agglomerated structure to porous structure with the increasing concentration of the oxidant. The magnetic ionic liquid, 1-butyl-3-methylimidazolium tetrachloroferrate (Bmim[$FeCl_4$]), played a major role of oxidant when the concentration was lower than 0.075*M*. As the concentration increased to 0.075*M*, the π–π interactions between pyrrole cations and iminazole ring of Bmim[$FeCl_4$], as evidenced by Fourier transform infrared spectrometer results, may affect the packing of PPy chains and subsequently cause the formation of porous structure of PPys. Electrochemical performances showed that PPy with porous structure displayed the highest specific capacitance of 170 F/g at a current density of 2 A/g in 1*M* H_2SO_4 solution and a good capacitive behavior, which has potential application as supercapacitor materials. © 2012 Wiley Periodicals, Inc. J. Appl. Polym. Sci. 000: 000–000, 2012

KEYWORDS: interfaces; conjugated polymers; electrochemistry; electron microscopy

Received 3 January 2012; accepted 23 April 2012; published online
DOI: 10.1002/app.37958

INTRODUCTION

In recent years, with growing demands for clean energy sources, electrochemical capacitors or supercapacitors have gained great concerns in many advanced power systems, such as digital communications, electric vehicles, burst power generation, and memory back-up devices. According to different energy-storage mechanisms, supercapacitors can be classified into two types: (1) electric double-layer capacitors based on carbon materials with high surface area and (2) faradic pseudocapacitors based on metal oxides and conducting polymers. Among faradic pseudocapacitor electrode materials, conducting polymers, such as polyaniline, polypyrrole (PPy), polythiophene, are considered as the most promising candidates because of their low cost, facile synthesis, flexibility, and high pseudocapacitance.

Microstructured/nanostructured conducting polymers with high surface area and high porosity give the good performances as the electrode materials for supercapacitors because of their distinctive characteristics of conducting pathways, surface interactions, and nanoscale dimensions. To date, a great number of microstructured/nanostructured conducting polymers, such as nanotubes, nanowires, nanorods, and nanofibers, can be prepared by various methods like rapid mixing polymerization,[1] interfacial polymerization,[2] *in situ* seeding polymerization,[3] dilute polymerization,[4] electrochemistry,[5] or using templates and surfactants.[6–8] Among these reported approaches, interfacial polymerization has been invented and developed to synthesize conducting polymer nanostructures in the past several years.[9–11] It is a general chemical route based on a polymerization reaction performed in an immiscible aqueous/organic biphasic system, with the monomer dissolved in the organic phase and the oxidant dissolved in the aqueous phase. The polymerization reaction starts at the interface (where the monomer contacts the oxidant), and subsequently, the resulting polymer migrates to the aqueous phase.

Among the conducting polymers, PPy, which consists of five-membered heterocyclic rings, stands out because of its good electrical conductivity, redox properties, and relatively good environmental stability. Very recently, various microstructured/nanostructured PPys, such as nanocapsules,[12] microfibers/nanofibers,[13,14] branched fibers,[15] coral-like structure,[16] and even nanoneedles,[17] have been successfully synthesized by interfacial polymerization with the aid of templates or surfactants.

However, porous PPy film polymerized by interfacial polymerization without surfactants or any acids is still challenging.

Recently, a magnetic ionic liquid, 1-butyl-3-methylimidazolium tetrachloroferrate (Bmim[$FeCl_4$]) is reported to be used as solvent for polymerization of nanostructured PPy.[18] Such imidazolium ionic liquids associated with specific anions are known to self-organize in a way that is adaptable to the fabrication of microstructures/nanostructures of conducting polymers and inorganic materials.[19,20] Kim et al.[18] presumed that the $FeCl_4$ moiety could play roles as a synthetic catalyst as well as a dopant, when polymerization of π-conjugated polymer was conducted in Bmim[$FeCl_4$]. In this study, Bmim[$FeCl_4$] is used as oxidant as well as pore generator for the interfacial polymerization of porous PPy films. The effect of the concentrations of Bmim[$FeCl_4$] on the morphology and electrochemical performance of PPys has been investigated. The structures of the PPys are characterized by scanning electron microscopy (SEM), atomic force microscopy (AFM), Fourier transform infrared spectrometer (FTIR), and X-ray diffraction (XRD) test. The electrochemical properties of the PPys are investigated by cyclic voltammetry (CV), galvanostatic charge–discharge, and electrochemical impedance spectroscopy (EIS) technology.

EXPERIMENTAL

Materials

Pyrrole (Sinopharm Chemical Reagent ,Shanghai, China) was purified by distillation under reduced pressure and stored in a refrigerator prior to use. Bmim[$FeCl_4$] and 1-butyl-3-methylimidazolium hexafluorophosphate (Bmim[PF_6]) were of analytical grade and purchased from Shanghai Chengjie Chemical Reagent Company (Shanghai, China). 1,5-Naphthalene disulfonic acid (1,5-NDA) and anthraquinone sulfonic acid (AQS) were of analytical grade and obtained from Sinopharm Chemical Reagent (Shanghai, China). All other reagents were of analytical grade and used as supplied without further purification.

Preparation of PPy

PPys were prepared by interfacial polymerization in *n*-hexane/water interface used Bmim[$FeCl_4$] as oxidant. It is noted that three samples of at each ratio were prepared to verify the reducibility. The concentrations of Bmim[$FeCl_4$] were varied as 0.025, 0.05, 0.075, and 0.1*M*, and the resulting polymers were designated as PPy1, PPy2, PPy3, and PPy4, respectively. The synthetic parameters are shown in Table I. In a typical preparation, a 1 mmol pyrrole (0.1*M*) was dissolved in 10 mL *n*-hexane as organic phase. Oxidant solution of 0.75 mmol Bmim[$FeCl_4$] (0.075*M*) was dissolved in 10 mL deionized water as water phase. Oxidant solution (water phase) was put first in 50-mL beaker, and on top of it, the monomer solution (the organic phase) was poured carefully with the help of a pipette, generating an interface between the organic phase and water phase. As shown in Figure 1, after a period of time, a gray color appears at the interface, followed by a black color typical of conducting form of PPy. Polymerization was carried out at the interface under static conditions for 24 h at room temperature, and a black self-supported film was collected at the interface. The film was washed with deionized water for three to four times and dried in a vacuum oven at 60°C for 24 h.

Table I. Synthetic Parameters of PPys

	$C_{(Bmim[FeCl4])}$ (*M*)	$C_{(pyrrole)}$ (*M*)
PPy1	0.025	0.1
PPy2	0.05	0.1
PPy3	0.075	0.1
PPy4	0.1	0.1

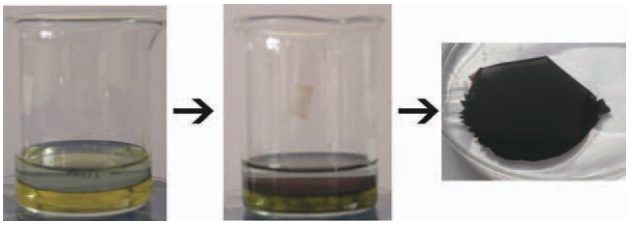

Figure 1. Scheme of the interfacial polymerization of PPys. [Color figure can be viewed in the online issue, which is available at wileyonlinelibrary.com.]

Characterization

The morphologies of the products were carried out using SEM (Hitachi S-4800, Tokyo, Japan). The specimens were platinum coated before examination. The surface morphology of the products was analyzed by AFM (5500, Agilent Technologies). FTIR spectra were recorded on a Bruker VECTOR22 FTIR spectrometer (Karlsruhe, Germany) using pressed KBr pellets. XRD patterns were measured using a Rigaku D/MAX-RC X-ray diffractometer (Tokyo, Japan) with Cu Kα radiation (λ = 0.1541 nm). The electrical conductivity measurements were conducted by the conventional four-probe technique at room temperature.

All electrochemical experiments were performed on a CHI660c electrochemical work station (Shanghai Chenhua Instruments Company, Shanghai, China) in a three-electrode system. Platinum foils and saturated calomel electrode were used as counter and reference electrodes, respectively. The same weight of the samples (5 mg) was used for the tests of electrochemical performances of PPys. The films connected by simple alligator clips were used as the working electrodes. The electrolyte was 1 mol/L H_2SO_4. CV tests were done between −0.8 and 0.2 V at a rate of 10 mV/s. Galvanostatic charge–discharge curves were measured at a current density of 0.5 A/g. EIS measurements were carried out in the frequency range from 10^5 to 0.01 Hz at open circuit potential with an ac perturbation of 5 mV.

RESULTS AND DISCUSSION

Morphology and Structure of PPys

The influence of the synthetic parameters, such as the concentration of Bmim[$FeCl_4$] and the addition of dopants, on the morphologies of the PPys have been investigated. The microstructures and surface morphology of as-prepared PPys are investigated by both SEM and AFM measurements. Figure 2 presents SEM and AFM images (inset) of PPys synthesized with different concentrations of Bmim[$FeCl_4$]. As shown in Figure 2(A,a), agglomerates of spheres are produced when the concentration of Bmim[$FeCl_4$] reaches 0.025*M*. The diameter sizes of the microspheres are ranged from 100 to 400 nm. As the

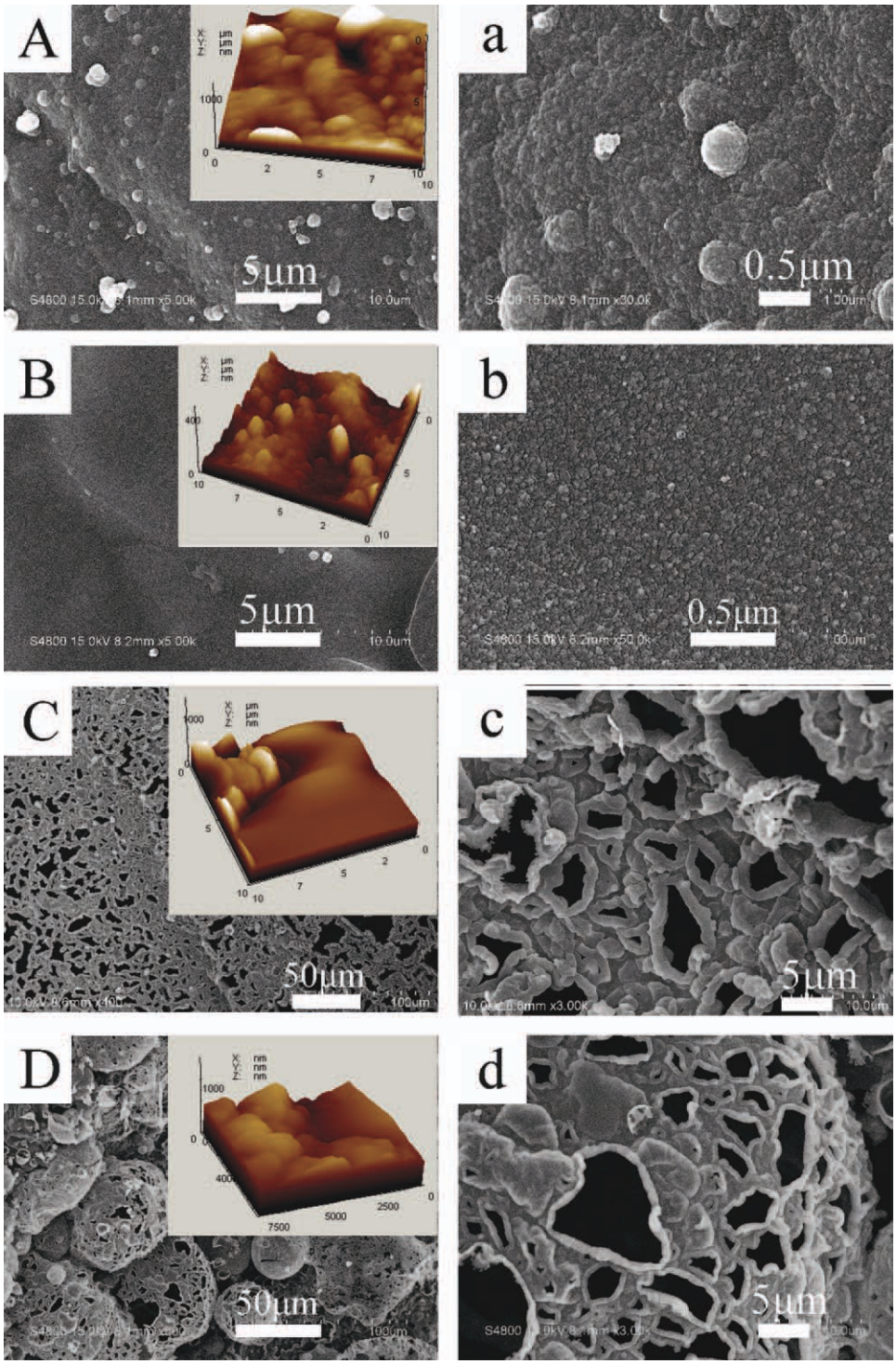

Figure 2. SEM and AFM images (inset) of PPys under the concentration of Bmim[$FeCl_4$]: (A,a) 0.025*M* (PPy1); (B,b) 0.05*M* (PPy2); (C,c) 0.075*M* (PPy3); and (D,d) 0.1*M* (PPy4). [Color figure can be viewed in the online issue, which is available at wileyonlinelibrary.com.]

concentration of Bmim[$FeCl_4$] increases to 0.05*M*, the resulting PPy is spherical in shape with an average diameter of 30–50 nm [Figure 2(B,b)]. Figure 2(A,a,B,b) shows dense agglomerates of PPy, and there is no evidence of pores. Interestingly, as the concentration of Bmim[$FeCl_4$] further increases to 0.075*M*, it is found that the synthesized PPy exhibits a novel porous morphology of aggregated PPy particles [Figure 2(C,c)]. The pore size changes from tens of micrometers to several hundred nanometers. As the concentration of Bmim[$FeCl_4$] increases to 0.1*M*, the resulting products are made up of small amount of PPy sheets and a large amount of PPy spheres [Figure 2(D)]. One can see that both PPy sheets and spheres still remain the porous

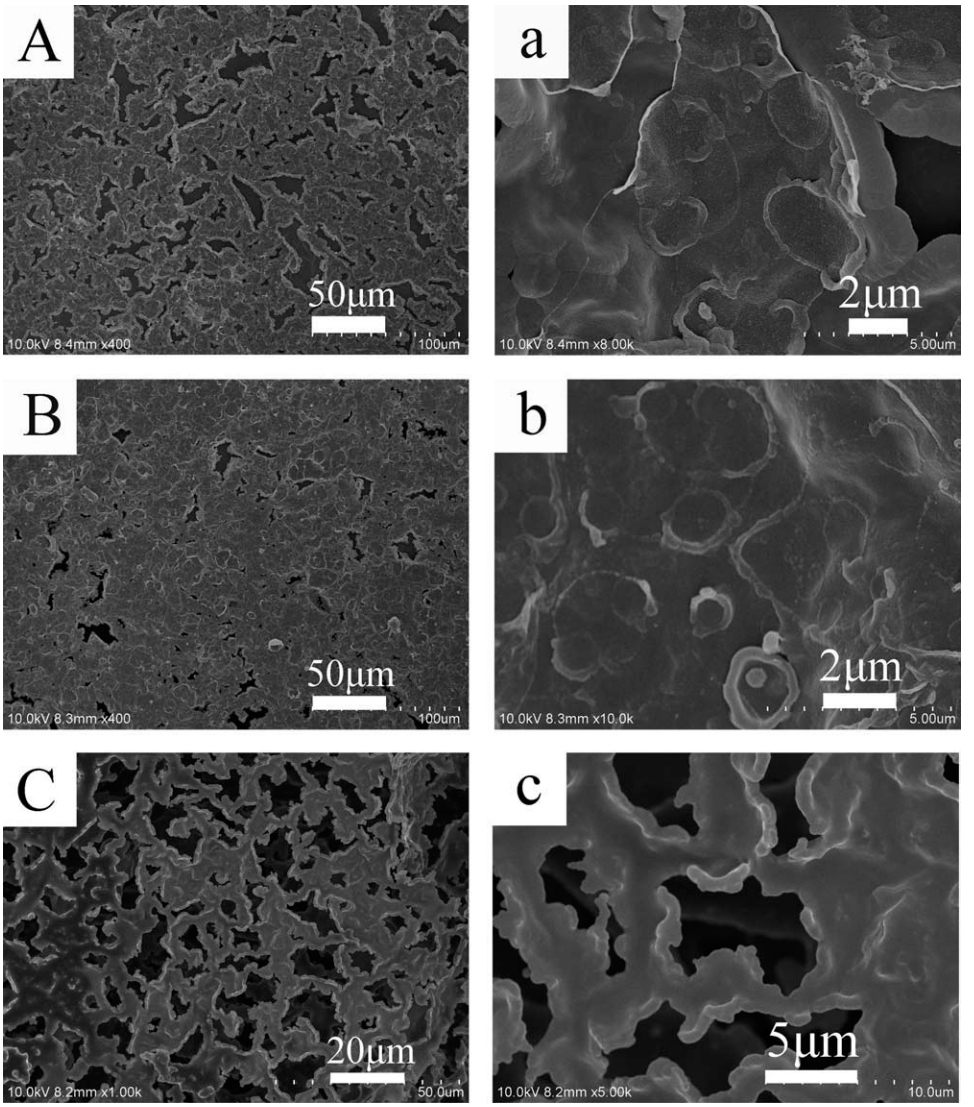

Figure 3. SEM images of PPy under 0.075*M* Bmim[$FeCl_4$]: (A,a) doped by 1,5-NDA; (B,b) doped by AQS; and (C,c) polymerized at water/Bmim[PF_6] interface.

structure. AFM was used to analyze the surface morphology of PPys, it can be seen from the inset images that compared with PPys porous structure (PPy3 and PPy4), PPys with dense structure (PPy1 and PPy2) showed relative smoother surfaces.

When the concentration of Bmim[$FeCl_4$] remains at 0.075*M*, the morphological changes of PPys in the presence of dopants and Bmim[PF_6] are observed in Figure 3. As can be seen from Figure 3(A,B), the numbers and size of the macropores are significantly decreased as the dopants are added. It is interesting to note that when either 1,5-NDA or AQS is used as the dopant for PPy, cyclic submicron-fiber structure is observed on the surface of PPy [Figure 3(a,b)]. Porous structure of PPy is also observed [Figure 3(C,c)], when water/Bmim[PF_6] interface is used for the preparation of PPy.

The FTIR spectra of the synthesized PPys are shown in Figure 4. FTIR of PPys revealed the characteristic peaks of PPy. Figure 4(e) shows FTIR spectra of the PPy powder synthesized by conventional *in situ* chemical polymerization used ammonium persulfate as oxidant in aqueous solution. It can be seen from Figure 4(e) that peaks located at 1561 and 1472 cm^{-1} are ascribed to the symmetric and antisymmetric pyrrole ring-stretching modes, respectively.[21] Peaks at 1290 and 1054 cm^{-1} are attributed to the =C—H in-plane vibration. The band situated at 1190 cm^{-1} is associated with the C—N stretching vibration.[22] The =C—H out-of-plane vibration is observed as the intensive band present at 929 cm^{-1}. PPy1 and PPy2 with aggregated microsphere morphology displayed a characteristic peaks of PPy, and no obvious shift is detected in Figure 4(a,b) compared with PPy powder [Figure 4(e)]. However, for PPy3 and PPy4 [Figure 4(c,d)], peaks at 1561, 1472, 1190, and 1054 cm^{-1} all shifted lower wavenumbers (downshifs of about 20–30 cm^{-1}). The spectra red-shifts phenomena could be ascribed to the strong π–π interaction and hydrogen bond between iminazole ring of Bmim[$FeCl_4$] and PPy backbone.[23] The band centered at 923 cm^{-1} assigning to the bipolaron state of PPy[24]

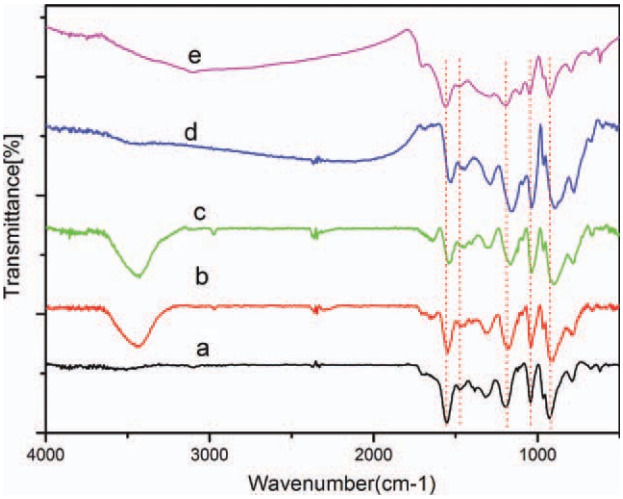

Figure 4. FTIR spectra of (a) PPy1; (b) PPy2; (c) PPy3; (d) PPy4; and (e) PPy powder. [Color figure can be viewed in the online issue, which is available at wileyonlinelibrary.com.]

shifted to lower wavenumbers (about 900 cm^{-1}) for PPy3 and PPy4. These shifts might be due to the increased π-electron density induced by charge transfer.[25]

Figure 5 presents the XRD patterns of the PPys synthesized by different concentrations of Bmim[$FeCl_4$] [Figure 5(a–d)] and PPy powder [Figure 5(e)]. A peak centered at about $2\theta = 25°$ is observed for all PPys, which is assigned as interplanar spacing of PPy chain structure.[26] The XRD patterns indicated that all the PPys were similar to PPy powder, and they were all basically amorphous materials. Thus, the molecular characterization of the resulting PPys confirmed that the concentration of the Bmim[$FeCl_4$] influenced the aggregations of PPy spheres, which led to changes in the PPys morphology, and did not have any effect on the PPy backbone and crystalline structure of the resulting polymer.

Formation Hypothesis of PPy with Porous Structure

In our study, the monomer pyrrole is distributed in *n*-hexane droplets. Pyrrole has better solubility in *n*-hexane but poor in water, so the monomer exists mainly in the oil phase. As the water-soluble oxidant (Bmim[$FeCl_4$]) was added, the monomer diffuses from the oil droplets toward the aqueous phase, the process of oxidant the opposite. Obviously, the interface of the oil droplet and the water is the necessary interface where the diffusing monomer encounters the oxidant existing in the water to initiate polymerization.

At the interface, pyrrole will form microsphere-like particles and attach to the growing PPy chains easily. These particles will grow continually at the interface when exposed to Bmim[$FeCl_4$].[27] As a low concentration of Bmim[$FeCl_4$] is added to the water phase, Bmim[$FeCl_4$] plays a major role of oxidant at the interface to initiate polymerization. As a result, aggregations of spherical granules formed at the oil/water interface. The ionic liquid can change the interactions between the pyrrole units, depending on the ionic liquid's concentration, and arranges them into different structures.[28] Thus, as the concentration of Bmim[$FeCl_4$] increases, the strong π–π interactions and hydrogen bond between pyrrole cations an iminazole ring of Bmim[$FeCl_4$] and PPy backbone, as evidenced by FTIR results, may cause the localization of pyrrole cations around the Bmim[$FeCl_4$] aggregations and subsequently affect the packing of PPy chains.[29,30] Such interactions may also account for the formation of porous structure of PPys.[31,32] When the concentrations of Bmim[$FeCl_4$] further increases, it is so-called secondary overgrowth lead to the globulation of the porous structure.[27] Because the aggregation state is formed by the π–π interactions and hydrogen bond, the PPy microstructures are not very compact. This can be supported by its XRD results (Figure 5), which is very similar to that of the PPy powder obtained by conventional approach.

Electrochemical Performances of PPys

Cyclic voltammetry was used in the determination of the electrochemical properties of the PPys. Figure 6 shows the CV curves of PPys electrode at a scan rate of 10 mV/s. The CV curves of PPy1, PPy3, and PPy4 all show roughly rectangular mirror images with respect to the zero-current line, indicating the excellent electrochemical behaviors. The CV curve of PPy2 electrode is distorted from the mirror image symmetry, suggesting that the reversibility of the PPy electrode is not good in the potential range. It can be seen that there are no redox peaks for all PPys in the working potential. As can be seen from Figure 6, the output currents of CV curves of PPy3 and PPy4 with porous structure are much larger than that of PPy1 and PPy2 with dense structure. As capacitance can be estimated from the output current divided by the scan rate, this indicates that the specific capacitances of the PPy3 and PPy4 are larger than that of PPy1 and PPy2. This improvement may be due to the porous structure as evidenced by SEM and higher conductivity of PPy3 (0.89 S/cm) and PPy4 (0.54 S/cm) than PPy1 (0.07 S/cm) and PPy2 (0.09 S/cm).

Figure 7 shows the charge–discharge curves of PPys. Accurate specific values of the PPys can be estimated from the discharge process according to the following equation:

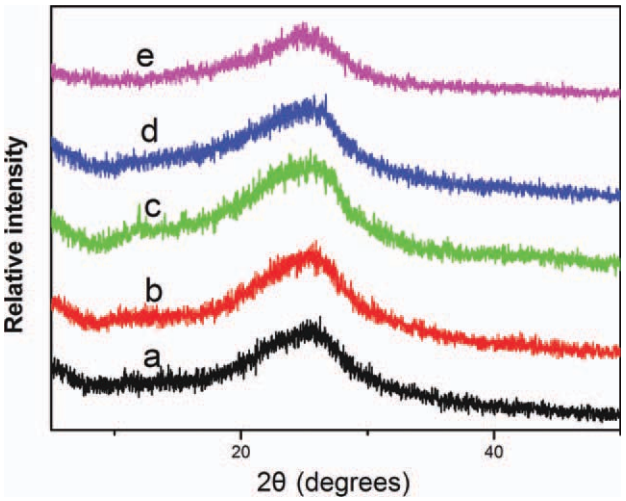

Figure 5. XRD patterns of (a) PPy1; (b) PPy2; (c) PPy3; (d) PPy4; and (e) PPy powder. [Color figure can be viewed in the online issue, which is available at wileyonlinelibrary.com.]

Applied Polymer SCIENCE

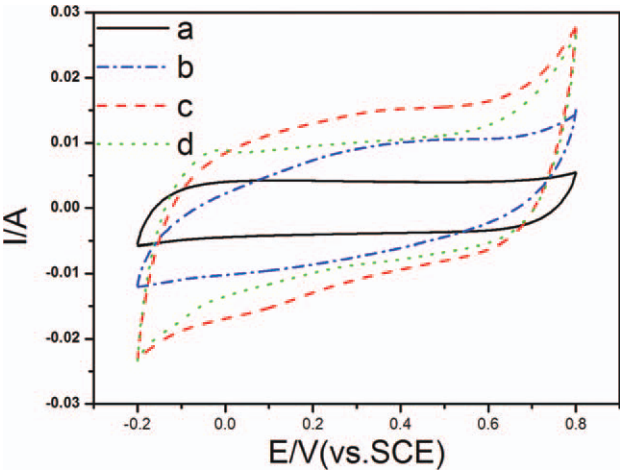

Figure 6. Cyclic voltammograms of (a) PPy1; (b) PPy2; (c) PPy3; and (d) PPy4. [Color figure can be viewed in the online issue, which is available at wileyonlinelibrary.com.]

$$Cm = \frac{C}{m} = \frac{I\Delta t}{\Delta V m} \quad (1)$$

where I is the current of discharge, Δt is the discharge time, m is the mass of the active material, ΔV is the potential drop in the discharge progress. In this article, the current density (I/m) we used is equal to 2 A/g. Based on the above equation, the specific capacitance of PPy1, PPy2, PPy3, and PPy4 are 52, 114, 170, and 166 F/g, respectively. The high specific capacitance values of PPy3 and PPy4 indicate that the porous structure would be responsible for the permeation of electrolyte within the electrode and the large capacity at high current densities.

Impedance spectroscopy is a powerful tool for mechanistic analysis of interfacial processes and for evaluation of rate constants, double-layer capacitance, and so forth. Figure 8 represents the Nyquist plots for PPys obtained at open circuit potentials. The semicircular portion, observed at higher frequencies, corresponds to electron-transfer-limited processes, whereas the linear part is characteristic of lower frequencies and represents the diffusional-limited electron-transfer processes. The semicircle of the plots of PPys is not obvious or could not be detected for PPys, probably due to the low faradaic resistances.[33] The internal resistance (Rs) could be evaluated from the point intersecting with the real axis in the range of high frequency. The Rs of PPy1, PPy2, PPy3, and PPy4 are approximately 1.3, 1.1, 0.8, and 1.6 Ω, respectively. The low Rs value of PPy3 can be ascribed to a low ohmic resistance between the electrode and the separator electrolyte. The imaginary part of the impedance spectra at low frequencies represents the capacitive behavior of the electrode and approaches a 90° vertical line in an ideal capacitor.[34] It can be seen that the imaginary parts of both PPy3 and PPy4 [Figure 8(c,d)] is almost perpendicular to the real part of resistance, indicating a mainly pure capacitive behavior.

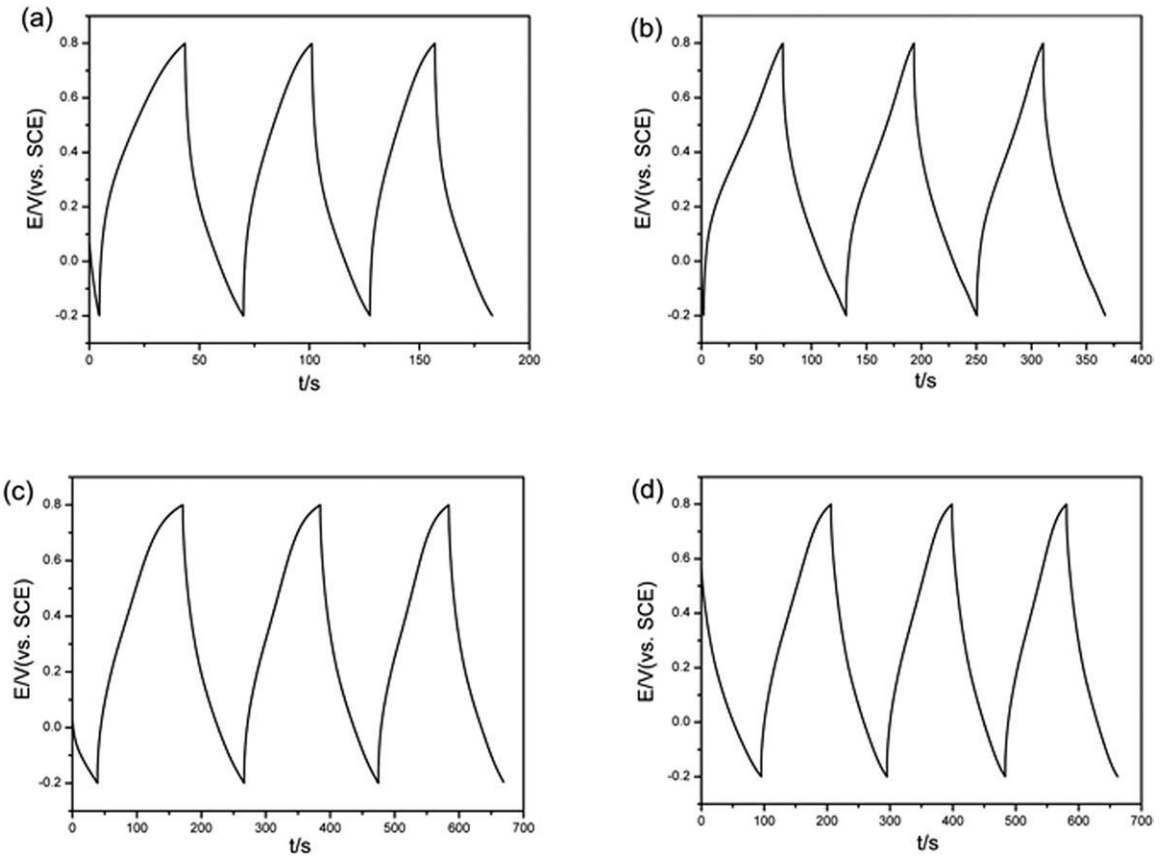

Figure 7. Galvastatic charge–discharge curve of (a) PPy1; (b) PPy2; (c) PPy3; and (d) PPy4.

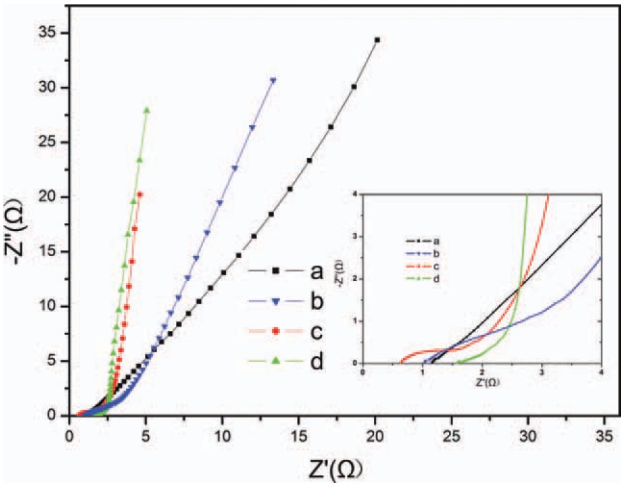

Figure 8. Nyquist plots of (a) PPy1; (b) PPy2; (c) PPy3; and (d) PPy4. [Color figure can be viewed in the online issue, which is available at wileyonlinelibrary.com.]

CONCLUSIONS

In summary, we have successfully synthesized porous structured PPy via a simple interfacial polymerization using Bmim[$FeCl_4$] as oxidant. The as-synthesized PPys showed dense microspherical/nanospherical agglomerated structure and porous structure with different concentrations of Bmim[$FeCl_4$]. Low concentration of Bmim[$FeCl_4$] in the interfacial reaction system only played a role oxidant. With the increase of the Bmim[$FeCl_4$] concentration, the strong π–π interactions and hydrogen bond between iminazole ring of Bmim[$FeCl_4$] and PPy backbone, as evidenced by FTIR results, may affect the packing of PPy chains and subsequently cause the formation of porous structure of PPys. Further increase of the Bmim[$FeCl_4$] concentration will lead to the globulation of the porous structure. A high specific capacitance of 170 F/g was obtained for PPy with porous structure at a current density of 2 A/g in 1*M* H_2SO_4 solution. CV curves and EIS spectra showed that PPy with porous structure displayed a good capacitive behavior. The electrochemical performances show that the PPy with porous structure has potential application as supercapacitor materials.

ACKNOWLEDGMENTS

This work was supported by National Natural Science Foundation of China (No. 21173120) and Postdoctoral Science Foundation of China (2012M511664) and Postdoctoral Science Foundation of Jiangsu Province (NO. 1102075C) and Hohai University (No. 2016-411108).

REFERENCES

1. Huang, J. X.; Kaner, R. B. *Angew. Chem. Int. Ed.* **2004,** *43*, 5817.
2. Huang, J. X.; Kaner, R. B. *J. Am. Chem. Soc.* **2004,** *126*, 851.
3. Tran, H. D.; Wang, Y.; Darcy, J. M.; Kaner, R. B. *ACS Nano* **2008,** *2*, 1841.
4. Subramania, A.; Devi, S. L. *Polym. Adv. Technol.* **2008,** *19*, 725.
5. Ghenaatian, H. R.; Mousavi, M. F.; Kazemi, S. H.; Shamsipur M. *Synth. Met.* **2009,** *159*, 1717.
6. Li, J. B.; Jia, Q. M.; Zhu, J. W., Zheng, M. S. *Polym. Int.* **2008,** *57*, 337.
7. Zhang, X.; Goux, W. J.; Manohar, S. K. *J. Am. Chem. Soc.* **2004,** *126*, 4502.
8. Wang, X.; Yang, C.; Liu, P. *Mater. Lett.* **2011,** *65*, 1448.
9. Li, D.; Huang, J.; Kaner, R. B. *Acc. Chem. Res.* **2008,** *42*, 135.
10. Li, D.; Kaner, R. B. *J. Am. Chem. Soc.* **2005,** *128*, 968.
11. Li, D.; Kaner, R. B. *J. Mater. Chem.* **2007,** *17*, 2279.
12. Zhang, L.; Liu, P.; Ju, L. L.; Wang, L.; Zhao, S. N. *Macromol. Res.* **2010,** *18*, 648.
13. Xing, S. X.; Zhao, G. K.; Yuan, Y. Polym. *Composite* **2008,** *29*, 22.
14. Goel, S.; Mazumdar, N. A.; Gupta, A. *Polym. Adv. Technol.* **2010,** *21*, 205.
15. Tamer, U.; Kanbes, C.; Ertas, N. *Int. J. Polym. Anal. Charact.* **2009,** *14*, 259.
16. Hou, L. R.; Yuan, C. Z.; Li, D. K.; Yang, L.; Shen, L. F.; Zhang, F.; Zhang X. G. *Electrochim. Acta* **2011,** *56*, 6049.
17. Nuraje, N.; Su, K.; Yang, N. L.; Matsui, H. *ACS Nano* **2008,** *2*, 502.
18. Kim, J. Y.; Kim, J. T.; Song, E. A.; Min, Y. K.; Hamaguchi, H. *Macromolecules* **2008,** *41*, 2886.
19. Rogers, R. D.; Seddon, K. R. *Science* **2003,** *302*, 792.
20. Pringle, J. M.; Ngamna, O.; Lynam, C.; Wallace, G. G.; Forsyth, M.; MacFarlane, D. R. *Macromolecules* **2007,** *40*, 2702.
21. Cho, G.; Fung, B. M.; Glatzhofer, D. T.; Lee, J. S.; Shul, Y. G. *Langmuir* **2001,** *17*, 456.
22. Oh, E. J.; Jang, K. S.; MacDiarmid, A. G. *Synth. Met.* **2002,** *125*, 267.
23. Bissessur, R.; Liu, P. K. Y.; Scully, S. F. *Synth. Met.* **2006,** *156*, 1023.
24. Liu, Y. C.; Lin, Y. T. *J. Phys. Chem. B* **2003,** *107*, 11370.
25. Zhang, W.; Wen, X.; Yang, S. *Langmuir* **2003,** *19*, 4420.
26. Cheah, K.; Forsyth, V. T.; Truong, V. T. *Synth. Met.* **1998,** *94*, 215.
27. Liu, S. W.; Zhu, K. Z.; Zhang, Y.; Xu, J. R. *Polymer,* **2006,** *47*, 7680.
28. Shang, S. M.; Li, L.; Yang, X. M.; Zheng, L. J. *Colloid Interface Sci.* **2009,** *333*, 415.
29. Lu, X.; Gao, H.; Chen, J.; Chao, D.; Zhang, W.; Wei, Y. *Nanotechnology* **2005,** *16*, 113.
30. Wang, X.; Liu, N.; Yan, X.; Zhang, W.; Wei, Y. *Chem. Lett.* **2005,** *34*, 42.
31. Zhou, Y.; Schattka, J. H.; Antonietti, M. *Nano Lett.* **2004,** *4*, 477.
32. Antonietti, M.; Kuang, D.; Smarsly, B.; Zhou, Y. *Angew. Chem. Int. Ed.* **2004,** *43*, 4988.
33. Wu, Q.; Xu, Y.; Yao, Z.; Liu, A.; Shi G. *ACS Nano* **2010,** *4*, 31963.
34. Conway, B. E. Electrochemical Supercapacitors, Scientific Fundamentals and Technological Applications; Kluwer Academic: New York, **1999.**